Review of Small-Signal Modeling Methods Including Frequency-Coupling Dynamics of Power Converters

Xiaolong Yue, *Member, IEEE*, Xiongfei Wang, *Senior Member, IEEE*, and Frede Blaabjerg, *Fellow, IEEE*

***Abstract*—Over the past years, the linearized modeling techniques for power converters have been continuously developed to capture the small-signal dynamics beyond half the switching frequency. This paper reviews and compares the small-signal modeling approaches based on a buck converter with voltage-mode control. The study includes the small-signal averaged modeling approach, the describing function method, and the harmonic state-space modeling approach, in order to be able to better select the correct method when modeling and analyzing a power electronic circuit as well as a power-electronic-based power system. The model comparison points out that the describing-function-based models do improve the modeling accuracy beyond the half-switching frequency of the converter, yet they fail to predict the frequency-coupling interactions (e.g., beat frequency oscillations) among multiple converters, and instead, harmonic state-space models in the multiple-input multiple-output form are required.**

***Index Terms*—Averaged model, crossed-frequency model, dc–dc converters, describing function, harmonic state space (HSS), small-signal modeling approach.**

I. Introduction

THE ubiquitous use of power electronic converters, ranging from milliwatt consumer electronics to gigawatt high-voltage direct current transmission systems [1]–[3], demands adequate dynamic models for stability analysis and controller design. In general, the switched-mode power converters with the closed-loop control are nonlinear time-discontinuous systems [4]. The linearization of converter dynamics is, thus, critical to utilize the classical feedback control theory for voltage/current regulations.

There are two general ways to deal with the time-discon tinuous dynamics of converters [5]–[10]. One way is to model the converter as a sampled-data system [5]–[7], and the other way is to apply the averaging theory to transform the converter as a time-continuous system [8]–[10]. The latter one is usually preferred to analyze the interaction with the continuous passive components in the system. The simplest averaging approach is to use the moving average operator [8]–[10], which is also known as the state-space averaging method, to average out the switching dynamics. However, the state-space averaging model is merely adequate for predicting the converter dynamics below half the switching frequency. To consider the switching ripple effect, two generalized averaging methods, i.e., Krylov–Bogoliubov–Mitropolsky (KBM) [11]–[14] and multifrequency averaging (MFA) [15]–[17], have thus been developed, and it was shown that the moving average operator is actually the first item of the KBM method and the index-0 (dc coefficient) of the MFA method [18].

The small-signal linearization refers to approximating a nonlinear system around a given operating point or a trajectory with small-signal perturbations [19]–[23]. The Taylor series is a fundamental tool for linearizing a continuous and differentiable nonlinear system [19]–[23]. The linearization around an equilibrium point gives a linear time-invariant (LTI) small-signal model, while the linearization around a time-periodic operating trajectory leads to a linear time periodic (LTP) small-signal model. In contrast to the linearization based on Taylor series, the harmonic linearization method based on Fourier series provides another way to linearize the small-signal model in the frequency domain [24]–[26].

The small-signal averaged model is a good tool for controller design, but its accuracy is questionable at high frequency because it eliminates the high-frequency information by the moving averaging. In voltage regulators, small-signal averaged models fail to predict the measured phase delay of the loop gain [27], [28]. In peak current mode control, the "current source" and averaged models [29]–[31] fail to explain the subharmonic oscillations. Then, the sideband effect introduced by pulsewidth modulation (PWM), switches, and analog-to-digital conversion is involved in the modeling. In voltage regulators, multifrequency small-signal models are proposed to explain the measured phase delay of the loop gain [27], [28]. According to the result obtained from discrete-time or sample-data models [6], [32], a modified averaged model [33] is proposed by adding the sample-and-hold effect to explain the subharmonic oscillation in peak current mode control. Since the modified average model applies only to constant frequency modulation converters, a new modeling approach based on the describing function concept is proposed in [34], which is applicable for both constant and variable frequency modulation current mode control. Based on the results of the describing function model, several

Manuscript received February 28, 2018; revised May 5, 2018; accepted June 9, 2018. Date of publication July 11, 2018; date of current version February 20, 2019. This work was supported by the VILLUM FONDEN under the VILLUM Investigators Grant-REPEPS. Recommended for publication by Associate Editor F. H. Khan. *(Corresponding author: Xiongfei Wang.)*

X. Yue was with the Department of Energy Technology, Aalborg University, 9220 Aalborg East, Denmark. He is now with Ericsson AB, 41756 Gothenburg, Sweden (e-mail: xiaolong_yue@163.com).

X. Wang and F. Blaabjerg are with the Department of Energy Technology, Aalborg University, 9220 Aalborg East, Denmark (e-mail: xwa@et.aau.dk; fbl@et.aau.dk).

Color versions of one or more of the figures in this paper are available online at http://ieeexplore.ieee.org.

Digital Object Identifier 10.1109/TPEL.2018.2848980

equivalent circuit models are proposed to predict the small-signal characteristics of average current mode control and V^2 control [35]–[37].

The small-signal averaged model provides a single-input single-output (SISO) linear relationship, and the describing-function-based models consider the sideband coupling to improve the accuracy of the SISO relationship to higher frequency regions. However, when analyzing the high-frequency interaction of multiple power converters in series or in parallel, the SISO model is questionable with respect to representing the high-frequency characteristics of switched power converters [38]–[41]. Under some high-frequency repetitive load transients, multiphase voltage regulators suffer from beat frequency oscillations of the phase currents [38]. In a dc nanogrid, the interaction of dc–dc converters with different switching frequencies can introduce beat frequency oscillations [39]–[41]. These facts indicate that in certain cases, the low-frequency sideband replaces the perturbation frequency and becomes the dominant component. The SISO models fail to explain the beat frequency oscillations. Then, crossed-frequency models are proposed in [38] and [41] to predict the beat frequency oscillations, which is a multiple-input multiple-output (MIMO) model describing the input to the output from a perturbation frequency not only to the perturbation frequency, but also to the sidebands of the perturbation frequency.

This paper reviews and compares the small-signal modeling methods. The linearization at an equilibrium point derives the small-signal averaged models. They are good tools for controller design, but their accuracy become questionable at high frequency. The harmonic linearization method gives the describing-function-based models, in which the sideband effect is considered. The describing-function-based models improve the modeling accuracy and successfully predict the subharmonic oscillations in current mode control. However, both small-signal averaged models and describing-function-based models are SISO models, and they fail to predict the frequency-coupling interactions (e.g., beat frequency oscillations) among multiple converters. According to the trajectory linearization [20] and the LTP theory [46]–[48], harmonic state-space (HSS) models with MIMO forms are proposed. HSS models can be applied to predict, e.g., beat frequency oscillations [38], [41], model a power electronic circuit when its switching harmonics are relatively high (e.g., six-pulse diode rectifiers [49], [50] and modular multiple-level converters [51]), and also replace the switching circuit in order to reduce the simulation time of a large power network [45]. The main disadvantage of HSS models is that the model order is high, so normally reduced-order HSS models, i.e., crossed-frequency models, are required.

The rest of this paper is organized as follows. Section II discusses the system description and averaging methods. Section III introduces the small-signal averaged modeling approach and its limitations. Section IV introduces the describing function method and its limitations. Section V introduces the HSS modeling approach and its limitations. Section VI compares different small-signal models, and Section VII gives the conclusion of this paper.

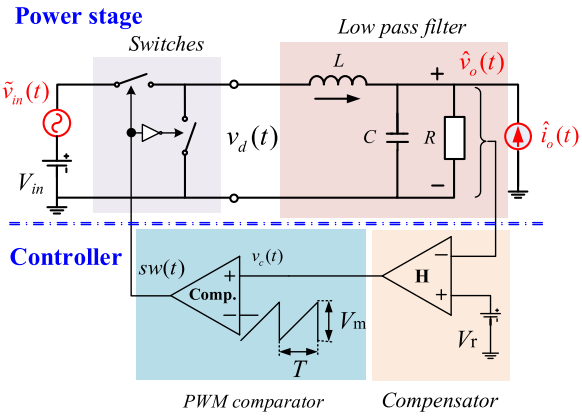

Fig. 1. Voltage-mode-controlled buck converter.

TABLE I
PARAMETERS OF THE POWER STAGE AND CONTROLLER IN FIG. 1

Description	Symbol	Value
Switching frequency	f_s	20 kHz
Input voltage	V_{in}	24 V
Output voltage	V_o	15 V
PWM gain	V_m	1
Inductor	L	1.1 mH
Output capacitor	C	47 μF
ESR of inductor	R_l	675 mΩ
ESR of output cap.	R_c	468 mΩ
Load resistor	R	20 Ω
Compensator	H	$\frac{279.2(1+0.0021s)(1+0.00034s)}{s(1+8.9\times10^{-6}s)(1+1.6\times10^{-5}s)}$

II. System Description and Modeling Foundation

Fig. 1 shows a closed-loop voltage-mode-controlled buck converter, and Table I lists the parameters of the power stage and controller (ESR represents the equivalent series resistance). The converter is used as an example for illustrating the principles of different modeling methods. Assume that the steady-state input voltage is a constant dc value, and the converter works in the continuous conduction mode. This topology is simple, but it embodies almost all the difficulties associated with the modeling of power electronic converters.

A. Switching Model of the Power Stage

For the power stage shown in Fig. 1, the switching model of the power stage can be expressed as

$$L\cdot\frac{di_L(t)}{dt}=\mathrm{sw}(t)\cdot v_{\mathrm{in}}(t)-v_o(t)$$
$$C\cdot\frac{dv_o(t)}{dt}=i_L(t)-\frac{v_o(t)}{R} \quad (1)$$

where $\mathrm{sw}(t)$ represents the switching function, which is

$$\mathrm{sw}\,(t) = \begin{cases} 0, & 0 \le t \le t_{\mathrm{on}} \\ 1, & t_{\mathrm{on}} \le t \le T. \end{cases} \tag{2}$$

When the duty ratio $D = t_{\mathrm{on}}/T_s$ (T_s is the switching period) is constant, $\mathrm{sw}(t)$ becomes $\mathrm{sw}_0(t)$, which is a steady state of the switching function. Using the Fourier transformation [51], $\mathrm{sw}_0(t)$ can be rewritten as

$$\mathrm{sw}_0(t) = D + \sum_{k\neq 0, k=-\infty}^{\infty} \frac{\sin(k\pi D)}{k\pi} e^{-jk\pi D} \cdot e^{-jk\omega_s t} \tag{3}$$

where $k \in Z$ (integer number) and $\omega_s = 2\pi/T_s$. Supposing

$$\vec{x}(t) = \begin{bmatrix} i_L(t) \\ v_o(t) \end{bmatrix}, \quad \mathbf{A} = \begin{bmatrix} 0 & -\dfrac{1}{L} \\ \dfrac{1}{C} & -\dfrac{1}{RC} \end{bmatrix}, \quad \mathbf{B} = \begin{bmatrix} \dfrac{1}{L} \\ 0 \end{bmatrix}$$

the switching model given in (1) can be expressed as

$$\frac{d}{dt}\vec{x}(t) = \mathbf{A} \cdot \vec{x}(t) + \mathbf{B} \cdot \mathrm{sw}(t) \cdot v_{\mathrm{in}}(t). \tag{4}$$

Considering the open-loop modulation only, the predefined switching function $\mathrm{sw}(t)$ can be seen as a time-varying coefficient, other than an input to the model. Hence, the switching model in (4) is linear but time-discontinuous varying [4]. However, in a closed-loop control system, the switching function $\mathrm{sw}(t)$ is determined by both state variables of the system and the clocking carrier waveform, which is an input of the switching model given in (4), and hence, the system becomes nonlinear and time-discontinuous varying [4].

Since most of the theories that have been developed are centered on linear systems, the way to make a nonlinear system to become a linear system is important. Taylor-series-based linearization is a commonly used method [19]–[21]. However, the switching model of a power converter is time discontinuous so that the Taylor series fails to be applied directly. Hence, averaging methods to transform a time-discontinuous system to a time-continuous model are required.

B. Averaging Methods

The basic idea of an averaged state-space approach is to average the several possible circuit configurations according to the ON- and OFF-states of the converter by a moving average operator [8]–[10]

$$\bar{x}(t) = \frac{1}{T}\int_{t-T}^{T} x(\tau)d\tau. \tag{5}$$

The moving average operator is a useful tool for modeling switched power converters, but it does not provide any information about the current and voltage waveform ripple, i.e., details within each switching cycle. Then, two generalized averaging methods, KBM method [11]–[14] and MFA method [15]–[17], are proposed to give an estimation of the switching ripple. In this paper, the MFA method is introduced as an example.

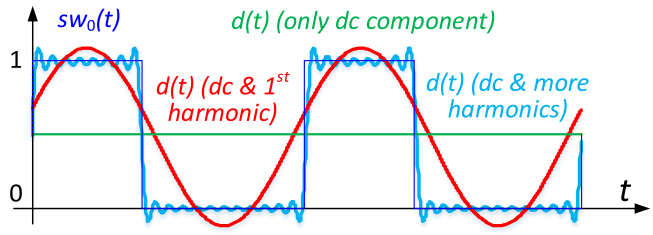

Fig. 2. MFA method—an example.

The MFA method [15], [16] is based on the fact that a waveform $x(t)$ can be approximated on the interval $\tau \in (t-T,\ T]$ to an arbitrary accuracy with a Fourier series representation of the form

$$x(\tau) = \sum_k \langle x\rangle_k(t) \cdot e^{jk\omega_s\tau} \tag{6}$$

where $k \in Z$, the sum is for all integers k, $\omega_s = 2\pi/T$, and $x_k(t)$ are complex Fourier coefficients. These coefficients $x_k(t)$ are functions of time, and they are given by

$$\langle x\rangle_k(t) = \frac{1}{T}\int_{t-T}^{T} x(\tau)e^{-jk\omega_s\tau}d\tau. \tag{7}$$

The kth coefficient of the Fourier series is also referred to as the index-k average or k-phasor [17]. Specifically, when $k = 0$, (7) becomes the moving average operator in (5), which indicates that the moving averaging is the index-zero average (dc coefficient) of the MFA method.

For the MFA equation in (6), the essence of the model reduction is to retain only the relatively large Fourier coefficients to capture the most important behavior of the system. For a fast switching circuit, we would retain only the index-zero (dc) coefficients to capture the low-frequency behavior. However, for slow switching or resonant converters, the index-k average, as well as the index-zero average, should be involved.

Fig. 2 shows the MFA method applied to the steady-state switching function $\mathrm{sw}_0(t)$ with different Fourier series. The accuracy of the averaged results $d(t)$ increases when more harmonics are involved.

Applying the averaging methods to the switching model of the power stage in (4), the averaged model can be expressed in a general form as

$$\begin{aligned} L\cdot\frac{di_L(t)}{dt} &= d(t)\cdot v_{\mathrm{in}}(t) - v_o(t) = f_1\left(d(t), v_{\mathrm{in}}(t), v_o(t)\right) \\ C\cdot\frac{dv_o(t)}{dt} &= i_L(t) - \frac{v_o(t)}{R} = f_2\left(i_L(t), v_o(t)\right) \end{aligned} \tag{8}$$

where $d(t)$ represents the averaged value of switching function $\mathrm{sw}(t)$, as shown in Fig. 2.

C. Linearization Techniques

Different linearization techniques lead to different small-signal models for the power stage. Fig. 3 shows the modeling foundations of small-signal averaged models, describing

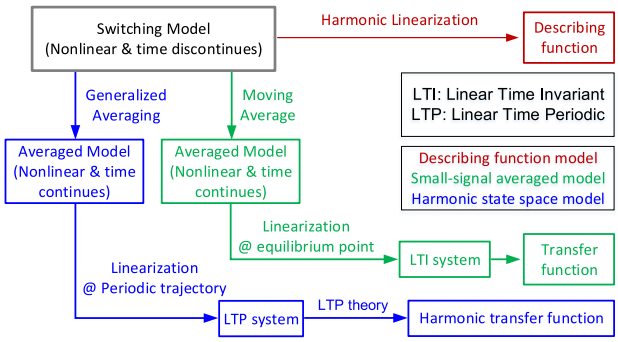

Fig. 3. Theoretical foundations of different small-signal models in power electronic circuits.

function methods, and HSS models. The small-signal averaged models are SISO LTI models derived through the linearization at an equilibrium point. The describing function models are derived from harmonic linearization, and they are also SISO models. HSS models are obtained by the linearization at a time-periodic trajectory and the LTP theory, which are MIMO LTI models.

III. Small-Signal Averaged Models

This section talks about small-signal averaged models of the voltage-mode-controlled buck converter in Fig. 1 and discusses the limitations of small-signal averaged models.

A. Small-Signal Averaged Models of the Power Stage

With the moving averaging method, an equilibrium point of (8) is the duty cycle D, the inductor current I_L, the input voltage $V_{\rm in}$, and the output voltage V_o. For the averaged model given in (8), supposing that the duty ratio has a small-signal perturbation, which is $d(t) = D + \tilde{d}(t)$. Similarly, define $i_L(t) = I_L + \tilde{i}_L(t)$, $v_{\rm in}(t) = V_{\rm in} + \tilde{v}_{\rm in}(t)$, and $v_o(t) = V_o + \tilde{v}_o(t)$, where $\tilde{d}(t)$, $\tilde{i}_L(t)$, $\tilde{v}_{\rm in}(t)$, and $\tilde{v}_o(t)$ are small-signal perturbations around D, I_L, $V_{\rm in}$, and V_o. The linearization of (8) based on the equilibrium point $(D, I_L, V_{\rm in}, V_o)$ gives

$$L\cdot\frac{d\tilde{i}_L(t)}{dt} = \left.\frac{\partial f_1}{\partial d}\right|_{\substack{d=D\\ v_{\rm in}=V_{\rm in}\\ v_o=V_o}}\cdot\tilde{d}(t) + \left.\frac{\partial f_1}{\partial v_{\rm in}}\right|_{\substack{d=D\\ v_{\rm in}=V_{\rm in}\\ v_o=V_o}}\cdot\tilde{v}_{\rm in}(t) - \left.\frac{\partial f_1}{\partial v_o}\right|_{\substack{d=D\\ v_{\rm in}=V_{\rm in}\\ v_o=V_o}}\cdot\tilde{v}_o(t)$$

$$C\cdot\frac{d\tilde{v}_o(t)}{dt} = \left.\frac{\partial f_2}{\partial i_L}\right|_{\substack{i_L=I_L\\ v_o=V_o}}\cdot\tilde{i}_L(t) - \left.\frac{\partial f_2}{\partial v_o}\right|_{\substack{i_L=I_L\\ v_o=V_o}}\cdot\tilde{v}_o(t) \quad (9)$$

which is further simplified as

$$L\cdot\frac{d\tilde{i}_L(t)}{dt} = V_{\rm in}\cdot\tilde{d}(t) + D\cdot\tilde{v}_{\rm in}(t) - \tilde{v}_o(t)$$

$$C\cdot\frac{d\tilde{v}_o(t)}{dt} = \tilde{i}_L(t) - \frac{1}{R}\cdot\tilde{v}_o(t) \quad (10)$$

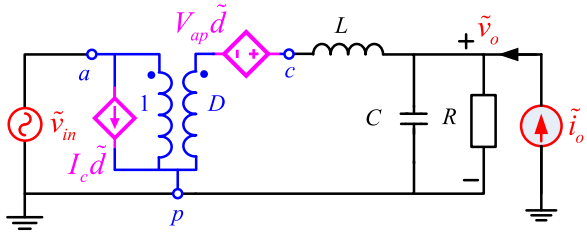

Fig. 4. Equivalent circuit of a buck converter by using the PWM switch model.

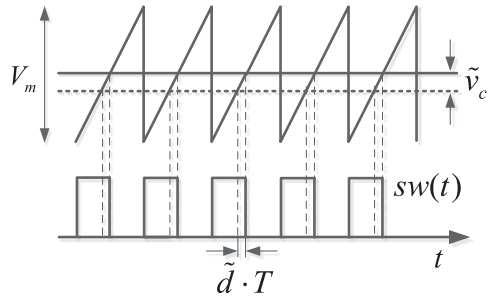

Fig. 5. Low-frequency gain of a PWM comparator (see Fig. 1).

where the coefficients are constant values, and thus, the small-signal model in (10) is an LTI model.

A small-signal state-space averaged model is obtained by writing (10) into a state-space form [8]–[10]. The small-signal state-space averaged model is actually derived from an averaging and linearization of the whole power stage. Doing the average for the nonlinear switching network only, rather than the whole converter, a three-terminal PWM switch model has been reported [53], [54]. Compared with the state-space averaged model, the PWM switch model is simpler and circuit-oriented with physical insights. Fig. 4 shows the equivalent circuit for the power stage of a buck converter using the PWM switch model.

From Fig. 4, the open-loop line-to-output transfer function $G_v(s)$, the open-loop output impedance $Z_{\rm op}(s)$, and control-to-output transfer function $G_d(s)$ can be derived as follows:

$$G_v(s) = \left.\frac{\tilde{v}_o(s)}{\tilde{v}_{\rm in}(s)}\right|_{\tilde{d}=0},\quad Z_{\rm op}(s) = \left.\frac{\tilde{v}_o(s)}{\tilde{i}_o(s)}\right|_{\tilde{d}=0},$$

$$G_d(s) = \left.\frac{\tilde{v}_o(s)}{\tilde{d}(s)}\right|_{\substack{\tilde{i}_o=0\\ \tilde{v}_{\rm in}=0}}. \quad (11)$$

B. Small-Signal Averaged Model for the PWM Comparator

The effect of the moving average operator in (5) can be approximated as a low-pass filter in the frequency domain. The averaged model captures mainly the dominant low-frequency characteristics of a dc–dc converter. If the input perturbation of the PWM comparator varies slowly compared with the switching frequency, then the input can be considered as a constant value within one switching period, as shown in Fig. 5.

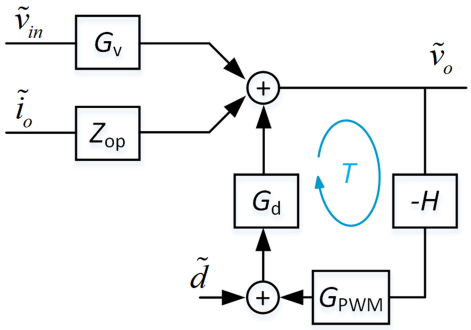

Fig. 6. Small-signal averaged model for a voltage-mode-controlled buck converter, as shown in Fig. 1.

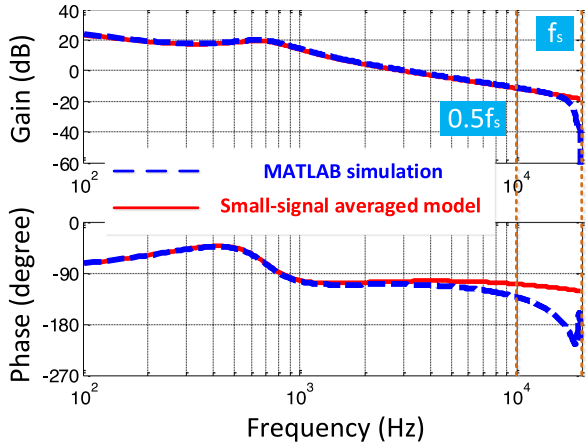

Fig. 7. Loop gain of a voltage-mode-controlled buck converter with switching frequency $f_s = 20$ kHz.

From Fig. 5, the low-frequency gain of the PWM comparator is

$$G_{\mathrm{PWM}} = \frac{\tilde{d}}{\tilde{v}_c} = \frac{1}{V_m}. \tag{12}$$

C. Small-Signal Averaged Model for Voltage-Mode-Controlled Buck Converters

Including the transfer function of the linear compensator, the small-signal averaged model of the converter can be obtained, as shown in Fig. 6. The closed-loop line-to-output transfer function, the output impedance, and the control-to-output transfer function can be derived as follows:

$$\frac{\tilde{v}_o(s)}{\tilde{v}_{\mathrm{in}}(s)} = \frac{G_v(s)}{1+T_{\mathrm{avg}}(s)}, \quad \frac{\tilde{v}_o(s)}{\tilde{i}_o(s)} = \frac{Z_{op}(s)}{1+T_{\mathrm{avg}}(s)}, \quad \frac{\tilde{v}_o(s)}{\tilde{d}(s)} = \frac{G_d(s)}{1+T_{\mathrm{avg}}(s)} \tag{13}$$

where $T_{\mathrm{avg}}(s) = G_d(s) \cdot G_{\mathrm{PWM}} \cdot H(s)$ is the loop gain of the small-signal averaged model.

D. Limitations of the Small-Signal Averaged Model

The small-signal averaged model is usually adequate for the controller design, but its accuracy is questionable at high frequencies, due to the ignorance of high-frequency dynamics by the moving averaging operator. In voltage regulators, the small-signal averaged model fails to predict the measured phase delay of the loop gain [27], [28]. In peak current mode control, the "current source" model and the averaged model [29]–[31] fail to explain the subharmonic oscillation phenomenon.

Fig. 7 shows the frequency response of the loop gain of a voltage-mode-controlled buck converter. Obviously, the small-signal model introduces phase lag in the high-frequency region, which is always below $-180°$ for any control bandwidth. However, the phase in real converters may be smaller than $-180°$ if the control bandwidth is too high [27]. This fact indicates that the small-signal averaged model has limitations when applied in the frequency region beyond one-tenth or one-sixth of the switching frequency.

IV. Describing Function Method

The inaccuracy of the small-signal averaged model at high frequencies is due to the sideband effect of the switching modulation process. To account for the sideband effect, the describing function method has been discussed to improve the modeling accuracy.

A. Sideband Effect in DC–DC Converters

Fig. 8 shows the sideband effect of a buck converter generated by the switches [39]. In Fig. 8(a), when the input voltage has a sinusoidal perturbation, the input and output voltage waveforms of the switching network are as shown in Fig. 8(b). The input voltage is expressed as

$$v_{\mathrm{in}}(t) = V_{\mathrm{in}} + \varepsilon \ \sin(\omega_x t + \theta). \tag{14}$$

Given the switching function $\mathrm{sw}(t) = \mathrm{sw}_0(t)$, the output voltage of the switching network is

$$\begin{aligned} v_d(t) &= \mathrm{sw}_0(t) \cdot v_{\mathrm{in}}(t) \\ &= DV_{\mathrm{in}} + D \cdot \varepsilon \ \sin(\omega_x t + \theta) \\ &\quad + 2V_{\mathrm{in}} \sum_{k=1}^{\infty} \frac{\sin(k\pi D)}{k\pi} \cos(k\omega_s t - k\pi D) \\ &\quad + \varepsilon \sum_{k=1}^{n} \frac{\sin(k\pi D)}{k\pi} [\sin(\omega_x + k\omega_s)t + \theta - k\pi D] \\ &\quad + \varepsilon \sum_{k=1}^{n} \frac{\sin(k\pi D)}{k\pi} [\sin(\omega_x - k\omega_s)t + \theta + k\pi D]. \end{aligned} \tag{15}$$

From (14) and (15), the frequency-domain waveforms of $v_{\mathrm{in}}(t)$ and $v_d(t)$ are shown in Fig. 8(c). The frequency-domain waveform of $v_d(t)$ contains not only the perturbation frequency

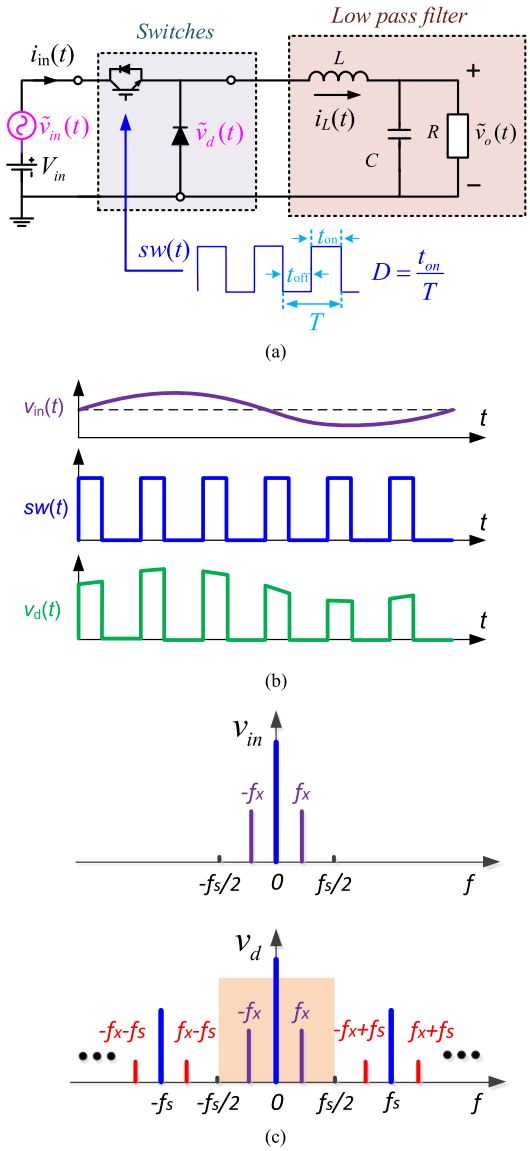

Fig. 8. Sideband effect generated by the switching. (a) Open-loop buck converter. (b) Time-domain waveforms of $v_{\rm in}(t)$, $\rm sw(t)$, and $v_d(t)$. (c) Frequency-domain magnitudes of $v_{\rm in}(t)$ and $v_d(t)$.

component, but also multiple additional frequency components, which are called sidebands.

Fig. 9 shows the time-domain waveforms and frequency-domain spectrum of a PWM comparator when the control voltage has a sinusoidal perturbation with frequency f_x. The output of the PWM comparator contains not only the perturbation frequency, but also sideband components [27], [40].

For a closed-loop-controlled converter, when the perturbation frequency is in the low-frequency regions, all sidebands are in the high-frequency regions, as shown in Figs. 8 and 9, which are well attenuated by the low-pass filter and the compensator. Therefore, the sideband effect can be ignored when the perturbation frequency is in the low-frequency regions. However, when the perturbation frequency is approaching to half of the switching frequency, a sideband is also approaching to the half

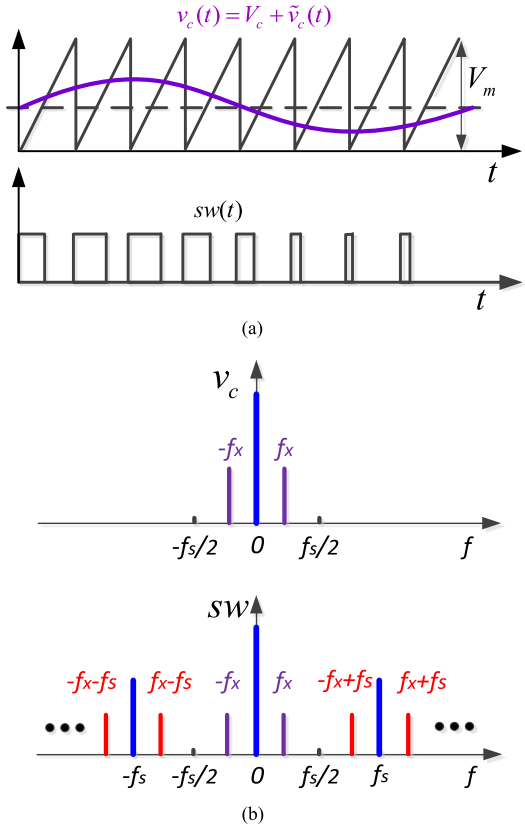

Fig. 9. Characteristic of a PWM comparator. (a) Time-domain waveforms. (b) Frequency-domain waveforms.

of the switching frequency, and hence, the sideband effect is nonnegligible. Since the small-signal averaged models ignore the sideband effect, their accuracy becomes questionable at the high frequencies.

B. Mathematical Foundations of the Describing Function Method

In contrast to the linearization of a nonlinear function in the time domain based on the Taylor series, the harmonic linearization is a linearization in the frequency domain based on the Fourier series [24]–[26]. The describing function refers to the equivalent gain or low-frequency gain defined by the harmonic linearization.

Generally, if the input to a nonlinear system is a sinusoidal function

$$u(t) = U \cdot \sin \omega t \tag{16}$$

the output of the nonlinear system $y(t) = g[(u(t))]$ can be represented by a Fourier series

$$\begin{aligned} y(t) &= \frac{A_0}{2} + \sum_{k=1}^{\infty} A_k \ \sin k\omega t + \sum_{k=1}^{\infty} B_k \ \cos k\omega t \\ &= \frac{A_0}{2} + \sum_{k=1}^{\infty} Y_k \ \sin\left(k\omega t + \phi_k\right) \end{aligned} \tag{17}$$

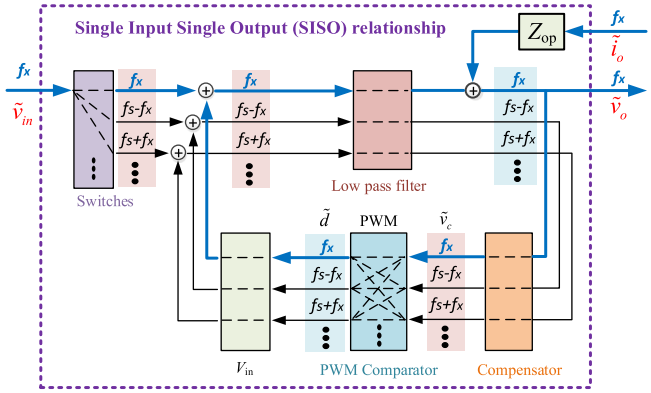

Fig. 10. Frequency-domain small-signal analysis of a voltage-mode-controlled buck converter.

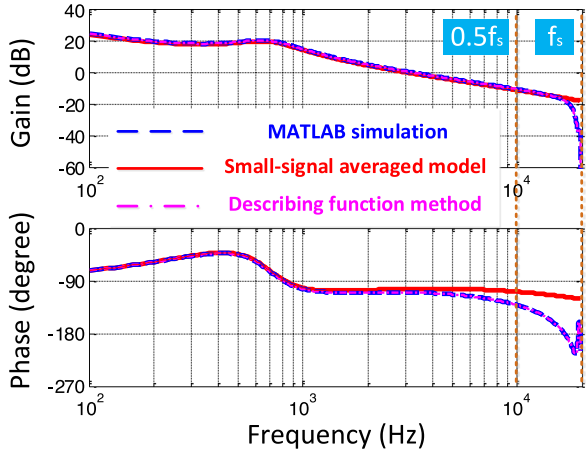

Fig. 11. Loop gain of a voltage-mode-controlled buck converter.

where

$$A_k = \frac{1}{\pi}\int_0^{2\pi} y(t)\cdot\cos\ k\omega t\cdot dt$$

$$B_k = \frac{1}{\pi}\int_0^{2\pi} y(t)\cdot\sin\ k\omega t\cdot dt$$

$$Y_k = \sqrt{A_k^2+B_k^2},\qquad \phi_k = \arctan\frac{A_k}{B_k}.$$

If the output can be approximated by its first-order term as

$$y(t)\approx Y_1\ \sin(\omega t+\phi_1) \tag{18}$$

then a describing function can be defined to represent the relationship between the input and output as the transfer function concept in an LTI system [24]–[26]. From (16) and (18), the describing function is expressed as

$$G = \frac{Y_1}{U}\angle\phi_1 = \frac{\sqrt{A_1^2+B_1^2}}{U}\angle\arctan\frac{A_1}{B_1}. \tag{19}$$

Note that the harmonic linearization can be applied directly to a switching model without averaging because the continuous differentiable condition is not required in the Fourier series [55].

C. Describing Function Method for the Closed-Loop-Controlled Converter

The describing function method provides an effective solution for modeling the sideband effect. Most of the PWM converters have a built-in low-pass filter to attenuate the high-frequency harmonics, which gives the foundation of harmonic linearization [26].

Fig. 10 shows the frequency-domain small-signal analysis of a voltage-mode-controlled buck converter by considering the sideband effect. The diagram becomes the small-signal averaged model in Fig. 6 if only the perturbation frequency component (marked by the bold blue line curves) is involved in the modeling. Since the describing functions, i.e., $v_o(f_x)/v_{\rm in}(f_x)$ and $v_o(f_x)/i_o(f_x)$, consider the frequency coupling in the switches and PWM, the modeling accuracy is improved compared with the small-signal averaged model.

In voltage-mode-controlled buck converters, the multifrequency small-signal model is proposed to explain the measured phase delay of the loop gain by considering the sideband effect of the PWM comparator [27]. The model gives a describing function for the loop gain of the converter, which is

$$T_{df}(f_x) = \frac{T_{\rm avg}(f_x)}{1+T_{\rm avg}(f_x-f_s)} \tag{20}$$

where $T_{\rm avg}(f)$ is the loop gain given by the small-signal averaged model in (13).

Fig. 11 shows loop gains of a voltage-mode-controlled buck converter obtained by simulation, small-signal averaged model, and describing function (multifrequency small-signal model). Compared with the transfer function derived by Fig. 6, the describing function derived by Fig. 10 considers the sideband effect and improves the modeling accuracy at high frequency.

D. Limitations of the Describing Function Method

With the describing function method, the accuracy of $v_o(f_x)/v_{\rm in}(f_x)$ and $v_o(f_x)/i_o(f_x)$ in Fig. 10 can be improved to several times of switching frequency [39], [40]. However, the describing function derives the reference input to the responded output only at the perturbation frequency. In the high-frequency region, the perturbation frequency component of the responded output may not be an accurate approximation for the responded output [40]. This limits the effective frequency regions of the describing function method.

In Fig. 8, when the small-signal perturbation is in the very low frequency regions ($0 < f_x \ll f_s/2$), the f_x component in $v_o(t)$ accurately approximates the responded output voltage perturbation because all the sidebands are in the high-frequency regions, and they are well attenuated by the low-pass filter. However, when the small-signal perturbation is in the high-frequency regions beyond half of the switching frequency (for example, $f_s/2 < f_x < f_s$), as shown in Fig. 12, the low-frequency component in $v_o(t)$ is at the sideband frequency $f_s - f_x$ rather than

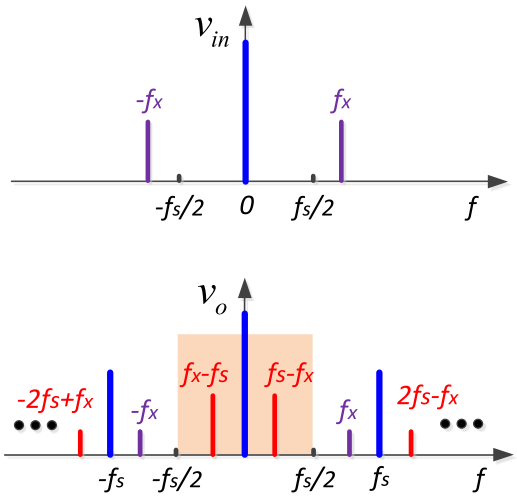

Fig. 12. Frequency-domain analysis of input and output voltages with perturbations on the condition in Fig. 8.

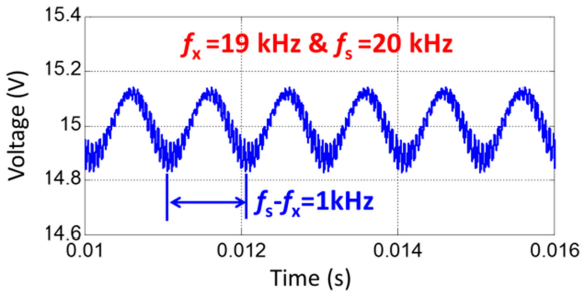

Fig. 13. Example of output voltage waveforms under a 19-kHz output current perturbation.

at the perturbation frequency f_x (note that $v_o(t)$ and $v_d(t)$ have same frequency components).

Fig. 13 shows the output voltage waveform of the closed-loop controlled converter in Fig. 1 when the output current has a perturbation with a frequency $f_x = 19$ kHz and the converter switching frequency is $f_s = 20$ kHz [40]. Obviously, the output voltage is dominant by the sideband component $f_s - f_x$ rather than the perturbation frequency component f_x, which means that the component $v_o(f_x)$ is no longer an accurate approximation of the responded output voltage. Therefore, although the describing function $v_o(f_x)/i_o(f_x)$ has a wideband accuracy from low frequency to several times of the switching frequency, $v_o(f_x)/i_o(f_x)$ is not always effective to describe the relationship between the injected output current perturbation and the corresponding output voltage response.

Under some high-frequency repetitive load transients, multiphase voltage regulators suffer from beat frequency oscillations of the phase currents [38]. In a dc nanogrid, the interaction of dc–dc converters with different switching frequencies introduces beat frequency oscillations [41]. These facts indicate that although the SISO describing-function-based models are effective for individual power converters at high frequencies, they are questionable to analyze the high-frequency interaction of multiple power converters in parallel or in series because the low-frequency sideband in such cases replaces the perturbation frequency and becomes dominant. Therefore, in order to predict the beat frequency oscillations, a crossed-frequency relationship between the perturbation frequency and the sidebands of the perturbation is required.

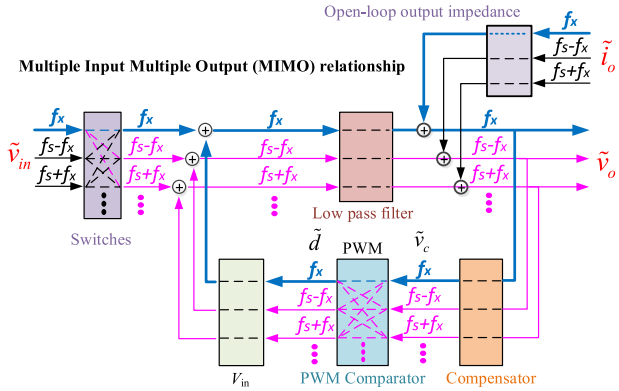

Fig. 14. MIMO relationship analysis for a voltage-mode-controlled buck converter.

V. Harmonic State-Space Models

Fig. 14 shows the frequency-domain analysis of a voltage-mode-controlled buck converter by considering the frequency coupling in the PWM comparator and switches. With a reference input (input voltage or output current) at the frequency f_x, the responded output voltage contains not only the f_x component, but also multiple sidebands. Basically, the relationship between the reference input and the responded output takes a MIMO form. In both the small-signal averaged model and the describing function model, the responded output voltage perturbation is approximated only by the component at the perturbation frequency, which simplifies the MIMO model into a SISO form. The diagram in Fig. 14 becomes the small-signal averaged model if only the perturbation frequency component (marked by the blue bold line curves) is involved in the modeling. When both the blue bold line curves and the pink line curves are considered, the diagram becomes the describing-function-based model.

The key in the modeling of the MIMO relationship in Fig. 14 is to express the multiple frequency coupling in the PWM comparator and switches effectively. Two challenges exist. First, the switching function becomes a time-varying trajectory rather than a dc working point because the switching harmonics are involved. Second, the definition of the crossed-frequency relationship between the perturbation frequency and the sidebands of perturbation, for example, $v_o(f_s - f_x)/i_o(f_x)$, is required.

A. Modeling Foundation: LTP Theory and Harmonic Transfer Function

1) LTP System and HSS: The linearization of a system around a time-varying trajectory gives a linear time-varying model [20]. For most of the fixed switching-frequency converters, their steady-state trajectories are time varying periodically,

and hence, the linearized model is an LTP model, which can be expressed by the following equation [46]–[48]:

$$\begin{aligned}\frac{dx(t)}{dt} &= A(t)\cdot x(t) + B(t)\cdot u(t)\\ y(t) &= C(t)\cdot x(t) + D(t)\cdot u(t)\end{aligned} \tag{21}$$

where $A(t)$, $B(t)$, $C(t)$, and $D(t)$ are periodic with a period T_s, which means $A(t+nT_s)=A(t)$ and similarly for $B(t)$, $C(t)$, and $D(t)$. The dynamic matrices of (21) can be expanded by Fourier series as

$$A(t) = \sum_{k=-\infty}^{+\infty} A_k e^{jk\omega_s t} \tag{22}$$

where $k \in Z$ and similarly for $B(t)$, $C(t)$, and $D(t)$. Since an LTP system maps a single harmonic into many harmonics, then it makes sense that the test signal includes all harmonics as well [46]. Supposing that the input of the LTP system, $u(t)$, is an exponentially modulated periodic (EMP) signal

$$u(t) = e^{st}\cdot \sum_{k=-\infty}^{+\infty} U_k e^{jk\omega_s t} \tag{23}$$

where $k \in Z$ and $s \in C$; the steady-state response of $x(t)$ and $y(t)$ are also EMP signals [46]

$$x(t) = e^{st}\cdot \sum_{k=-\infty}^{+\infty} X_k e^{jk\omega_s t}, \quad y(t) = e^{st}\cdot \sum_{k=-\infty}^{+\infty} Y_k e^{jk\omega_s t}. \tag{24}$$

The LTP system model in (21) can then be expanded in terms of Fourier series. With the principle of harmonic balance, the LTP model in (21) can be expressed as an infinite-dimensional matrix equation

$$\begin{aligned} s\mathbf{X} &= (\mathbf{A}-\mathbf{N})\,\mathbf{X} + \mathbf{B}\mathbf{U}\\ \mathbf{Y} &= \mathbf{C}\mathbf{X} + \mathbf{D}\mathbf{U}.\end{aligned} \tag{25}$$

In (25), state variables $\boldsymbol{X}$, $\boldsymbol{U}$, and $\boldsymbol{Y}$ are defined as the doubly infinite vectors representing the harmonic of the state, input, and output in terms of their Fourier coefficients X_k, U_k, and Y_k

$$\mathbf{X} = \begin{bmatrix} \vdots \\ X_{-1}(s-j\omega_s) \\ X_0(s) \\ X_1(s+j\omega_s) \\ \vdots \end{bmatrix}, \quad \mathbf{U} = \begin{bmatrix} \vdots \\ U_{-1}(s-j\omega_s) \\ U_0(s) \\ U_1(s+j\omega_s) \\ \vdots \end{bmatrix},$$

$$\mathbf{Y} = \begin{bmatrix} \vdots \\ Y_{-1}(s-j\omega_s) \\ Y_0(s) \\ Y_1(s+j\omega_s) \\ \vdots \end{bmatrix}. \tag{26}$$

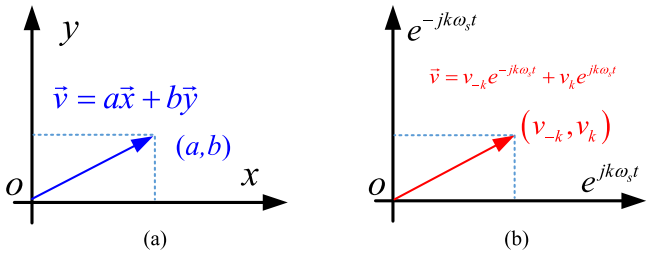

Fig. 15. Comparison of a 2-D plane and a 2-D HSS. (a) With base vectors $\vec{x}$ and $\vec{y}$. (b) With base vectors $e^{-jk\omega_s t}$ and $e^{jk\omega_s t}$.

The T-periodic matrix $A(t)$ is expressed in terms of its Fourier coefficients $(A_k, k \in Z)$, as a doubly infinite block Toeplitz matrix, which is a matrix with constant elements, and it can be expressed by

$$\mathbf{A} = \begin{bmatrix} \ddots & \vdots & \vdots & \vdots & \\ \cdots & A_0 & A_{-1} & A_{-2} & \cdots \\ \cdots & A_1 & A_0 & A_{-1} & \cdots \\ \cdots & A_2 & A_1 & A_0 & \cdots \\ & \vdots & \vdots & \vdots & \ddots \end{bmatrix}. \tag{27}$$

$B(t)$, $C(t)$, and $D(t)$ are with a similar definition in terms of their Fourier coefficients represented by B_k, C_k, and D_k $(k \in Z)$, and $\mathbf{N}$ is a diagonal matrix defined as

$$\mathbf{N} = \mathrm{diag}[\ldots, -jk\omega_s, \ldots, -j\omega_s, 0, j\omega_s, \ldots, jk\omega_s, \ldots]^T. \tag{28}$$

The infinite-dimensional matrix equation in (25) is called an HSS model [46].

Fig. 15 shows a comparison of a two-dimensional (2-D) plane and a 2-D HSS to illustrate the meaning of HSS. In the 2-D plane, as shown in Fig. 15(a), a vector can be represented by a vector (a, b) by the orthogonal base vectors $\vec{x}$ and $\vec{y}$ of the 2-D plane, where $a, b \in R$. Similarly, since the complex exponential functions $e^{jk\omega_s t}$ $(k \in Z)$ used in Fourier series are also orthogonal, a signal can also be represented by a vector that consists of its Fourier coefficients. Fig. 15(b) shows a 2-D HSS, in which a signal is expressed by a vector with its Fourier coefficients. When the HSS in Fig. 15(b) is extended to infinite dimensions, it becomes the HSS, as given in (25).

2) Definition of the Harmonic Transfer Function: The harmonic transfer function (HTF) [46]–[48] describes the input-to-output relationship through the Fourier coefficients of the input signal and those of the output signal, which is expressed as

$$\mathbf{Y} = \mathbf{G}(s)\mathbf{U} \tag{29}$$

where $\mathbf{G}(s) = \mathbf{C}[s\mathbf{I} - (\mathbf{A} - \mathbf{N})]^{-1}\mathbf{B} + \mathbf{D}$ ($\boldsymbol{I}$ represents the identity matrix), and it takes the form

$$\mathbf{G}(s) = \begin{bmatrix} \ddots & \vdots & \vdots & \vdots & \\ \cdots & G_0(s-j\omega_s) & G_{-1}(s) & G_{-2}(s+j\omega_s) & \cdots \\ \cdots & G_1(s-j\omega_s) & G_0(s) & G_{-1}(s+j\omega_s) & \cdots \\ \cdots & G_2(s-j\omega_s) & G_1(s) & G_0(s+j\omega_s) & \cdots \\ & \vdots & \vdots & \vdots & \ddots \end{bmatrix}.$$

The HTF represents the input–output relationship of an LTP system.

B. HSS Model for a Voltage-Mode-Controlled Buck Converter

For the buck converter shown in Fig. 1, with the generalized averaging method, a steady-state trajectory is the duty ratio function $d_s(t)$, inductor current $i_{Ls}(t)$, input voltage $v_{\mathrm{ins}}(t)$, and output voltage $v_{os}(t)$. Supposing the duty ratio function has a small-signal perturbation around its steady state, which is $d(t) = d_s(t) + \tilde{d}(t)$. Similarly, define $i_L(t) = i_{Ls}(t) + \tilde{i}_L(t)$, $v_{\mathrm{in}}(t) = v_{\mathrm{ins}}(t) + \tilde{v}_{\mathrm{in}}(t)$, and $v_o(t) = v_{os}(t) + \tilde{v}_o(t)$, where $\tilde{d}(t)$, $\tilde{i}_L(t)$, $\tilde{v}_{\mathrm{in}}(t)$, and $\tilde{v}_o(t)$ are small-signal perturbations around the steady-state trajectory. The linearization of (8) based on the steady-state trajectory ($d_s(t)$, $i_{Ls}(t)$, $v_{\mathrm{ins}}(t)$, and $v_{os}(t)$) is

$$\begin{aligned} L\cdot\frac{d\tilde{i}_L(t)}{dt} &= \left.\frac{\partial f_1}{\partial d}\right|_{\substack{d(t)=d_s(t)\\ v_{\mathrm{in}}(t)=v_{ins}(t)\\ v_o(t)=v_{os}(t)}}\cdot\tilde{d}(t) + \left.\frac{\partial f_1}{\partial v_{\mathrm{in}}}\right|_{\substack{d(t)=d_s(t)\\ v_{\mathrm{in}}(t)=v_{ins}(t)\\ v_o(t)=v_{os}(t)}} \\ &\quad\cdot\tilde{v}_{\mathrm{in}}(t) - \left.\frac{\partial f_1}{\partial v_o}\right|_{\substack{d(t)=d_s(t)\\ v_{\mathrm{in}}(t)=v_{ins}(t)\\ v_o(t)=v_{os}(t)}}\cdot\tilde{v}_o(t) \\ C\cdot\frac{d\tilde{v}_o(t)}{dt} &= \left.\frac{\partial f_2}{\partial v_o}\right|_{\substack{i_L(t)=i_{Ls}(t)\\ v_o(t)=v_{os}(t)}}\cdot\tilde{v}_o(t) - \left.\frac{\partial f_2}{\partial i_L}\right|_{\substack{i_L(t)=i_{Ls}(t)\\ v_o(t)=v_{os}(t)}} \\ &\quad\cdot\tilde{i}_L(t) \end{aligned} \tag{30}$$

which can be simplified as

$$\begin{aligned} L\cdot\frac{d\tilde{i}_L(t)}{dt} &= v_{\mathrm{ins}}(t)\cdot\tilde{d}(t) + d_s(t)\cdot\tilde{v}_{\mathrm{in}}(t) - \tilde{v}_o(t) \\ C\cdot\frac{d\tilde{v}_o(t)}{dt} &= \frac{1}{R}\cdot\tilde{v}_o(t) - \tilde{i}_L(t). \end{aligned} \tag{31}$$

In (31), the coefficients are constant or time varying periodically, and thus, this small-signal model is an LTP model. When writing (31) in an HSS form, the small-signal perturbations $\tilde{i}_L(t)$, $\tilde{v}_o(t)$, $\tilde{d}(t)$, and $\tilde{v}_{\mathrm{in}}(t)$ are represented by vectors, that are similarly defined as $\boldsymbol{X}$ in (26), the coefficients $d_s(t)$ and $v_{\mathrm{ins}}(t)$ are expressed as Toeplitz matrices, which are similarly defined as $\boldsymbol{A}$ in (27), and constant values L and C become $L\cdot\boldsymbol{I}$ and $C\cdot\boldsymbol{I}$ ($\boldsymbol{I}$ represents the identity matrix).

Fig. 16 shows the model to derive the HSS model of voltage-mode-controlled buck converters according to the relationship in Fig. 14, where $\boldsymbol{G_{\mathrm{sw}}}$ represents the HTF of the switching network, $\boldsymbol{G_{\mathrm{PWM}}}$ represents the HTF of the PWM comparator,

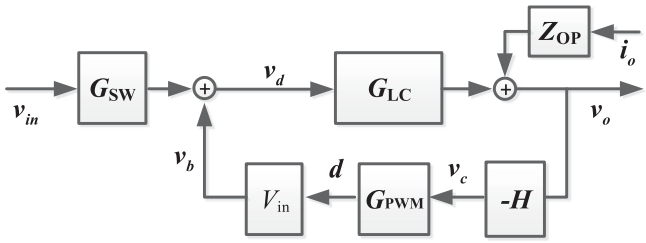

Fig. 16. Block diagram for HSS modeling of the system in Fig. 14.

$\boldsymbol{Z_{\mathrm{op}}}$ represents the HTF of the open-loop impedance, $\boldsymbol{G_{\mathrm{LC}}}$ represents the HTF of the *LC* low-pass filter, $\boldsymbol{H}$ represents the HTF of the compensator, and variables $\boldsymbol{v_{\mathrm{in}}}$, $\boldsymbol{i_{\mathrm{o}}}$, $\boldsymbol{d}$, and $\boldsymbol{v_{\mathrm{o}}}$ are small-signal input voltage perturbation, output current perturbation, switching function perturbation, and output voltage perturbation respectively.

According to the theory of the LTP system and HSS, $\boldsymbol{G_{\mathrm{sw}}}$ is expressed by Fourier coefficients of the duty ratio function $d_s(t)$. From (3), when considering first n items ($n \in Z$), $\boldsymbol{G_{\mathrm{sw}}}$ is expressed as [39]

$$\boldsymbol{G_{\mathrm{SW}}} = \begin{bmatrix} \ddots & \vdots & \vdots & \vdots & \\ \cdots & D & \frac{\sin\pi D}{\pi}e^{j\pi D} & \frac{\sin\pi D}{\pi}e^{j2\pi D} & \cdots \\ \cdots & \frac{\sin\pi D}{\pi}e^{-j\pi D} & D & \frac{\sin\pi D}{\pi}e^{j\pi D} & \cdots \\ \cdots & \frac{\sin\pi D}{\pi}e^{j2\pi D} & \frac{\sin\pi D}{\pi}e^{-j\pi D} & D & \cdots \\ & \vdots & \vdots & \vdots & \ddots \end{bmatrix}. \tag{32}$$

From [27] and [40], the HTF of the PWM comparator $\boldsymbol{G_{\mathrm{PWM}}}$ is expressed as

$$\boldsymbol{G_{\mathrm{PWM}}} = \frac{1}{V_m}\cdot\begin{bmatrix} \ddots & \vdots & \vdots & \vdots & \\ \cdots & 1 & e^{j2D\pi} & e^{j4D\pi} & \cdots \\ \cdots & e^{-j2D\pi} & 1 & e^{j2D\pi} & \cdots \\ \cdots & e^{-j4D\pi} & e^{-j2D\pi} & 1 & \cdots \\ & \vdots & \vdots & \vdots & \ddots \end{bmatrix}. \tag{33}$$

Supposing that $Z_{\mathrm{op}}(s)$ is the transfer function of the open-loop impedance, $G_{LC}(s)$ is the transfer function of the *LC* low-pass filter, and $H(s)$ is the transfer function of the compensator. Then, HTFs $\boldsymbol{Z_{\mathrm{op}}}$, $\boldsymbol{G_{\mathrm{LC}}}$, and $\boldsymbol{H}$ are diagonal matrices, which are

$$\mathbf{Z_{op}}(s) = \begin{bmatrix} \ddots & \vdots & \vdots & \vdots & \\ \cdots & Z_{\mathrm{op}}(s-j\omega_s) & 0 & 0 & \cdots \\ \cdots & 0 & Z_{\mathrm{op}}(s) & 0 & \cdots \\ \cdots & 0 & 0 & Z_{\mathrm{op}}(s+j\omega_s) & \cdots \\ & \vdots & \vdots & \vdots & \ddots \end{bmatrix}. \tag{34}$$

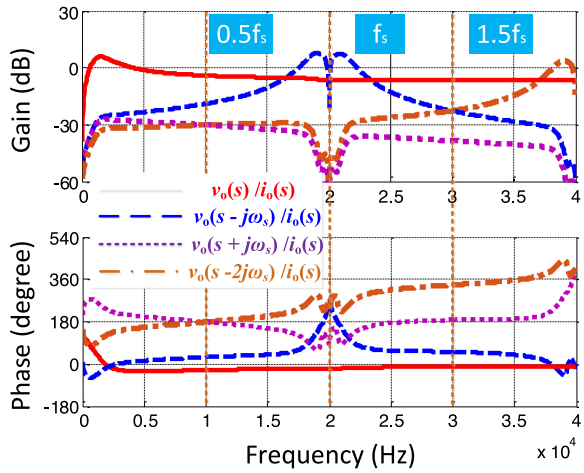

Fig. 17. Frequency characteristics of four HTFs of the closed-loop output impedance.

$$\boldsymbol{G_{\mathrm{LC}}}(s)=\begin{bmatrix} \ddots & \vdots & \vdots & \vdots & \\ \cdots & G_{\mathrm{LC}}(s-j\omega_s) & 0 & 0 & \cdots \\ \cdots & 0 & G_{\mathrm{LC}}(s) & 0 & \cdots \\ \cdots & 0 & 0 & G_{\mathrm{LC}}(s+j\omega_s) & \cdots \\ & \vdots & \vdots & \vdots & \ddots \end{bmatrix} \tag{35}$$

$$\boldsymbol{H}(s)=\begin{bmatrix} \ddots & \vdots & \vdots & \vdots & \\ \cdots & H(s-j\omega_s) & 0 & 0 & \cdots \\ \cdots & 0 & H(s) & 0 & \cdots \\ \cdots & 0 & 0 & H(s+j\omega_s) & \cdots \\ & \vdots & \vdots & \vdots & \ddots \end{bmatrix}. \tag{36}$$

Variables in Fig. 16, for example $\boldsymbol{i_o}$ and $\boldsymbol{v_o}$, are vectors in the HSS, which are

$$\boldsymbol{i}_o(s)=\begin{bmatrix} \vdots \\ i_o(s-j\omega_s) \\ i_o(s) \\ i_o(s+j\omega_s) \\ \vdots \end{bmatrix}, \boldsymbol{v}_o(s)=\begin{bmatrix} \vdots \\ v_o(s-j\omega_s) \\ v_o(s) \\ v_o(s+j\omega_s) \\ \vdots \end{bmatrix}. \tag{37}$$

From Fig. 16, the HTF of the closed-loop output impedance $\boldsymbol{Z_{\mathrm{ocl}}}$ can be derived as [40]

$$\boldsymbol{v}_o(s)=\boldsymbol{Z}_{\mathrm{ocl}}(s)\times\boldsymbol{i}_o(s)$$

$$\boldsymbol{Z}_{\mathrm{ocl}}=(\boldsymbol{I}+\boldsymbol{G}_{\mathrm{LC}}\times V_{\mathrm{in}}\times G_{\mathbf{PWM}}\times\boldsymbol{H})^{-1}\times\boldsymbol{Z}_{\mathrm{op}}. \tag{38}$$

Fig. 17 shows the frequency characteristics of four HTFs of $\boldsymbol{Z_{\mathrm{ocl}}}$, in which $s=j\cdot 2\pi f_x$. With an output current perturbation at frequency f_x, the component at perturbation frequency f_x and three sidebands f_x-f_s, f_x+f_s, and f_x-2f_s in the output voltage are considered in Fig. 17. Note that the diagonal HTF (the blue solid line) is the same as the result obtained by the describing function model.

From Fig. 17, it is reasonable to approximate the output voltage by only the component with perturbation frequency when the frequency of the output current perturbation is in the low-frequency regions. However, in the high-frequency regions, especially the regions around the switching frequency, the low-frequency sideband has a very large magnitude, so it is questionable to approximate the responded output by only the component at the perturbation frequency.

As a conclusion from Fig. 17, in the low-frequency regions, the SISO output impedance is adequate for capturing the relationship between the output current perturbation $\tilde{i}_o$ and the output voltage perturbation $\tilde{v}_o$, but in the high-frequency regions especially around the switching frequency, the relationship between $\tilde{i}_o$ and $\tilde{v}_o$ should be described by the MIMO HSS output impedance matrix model.

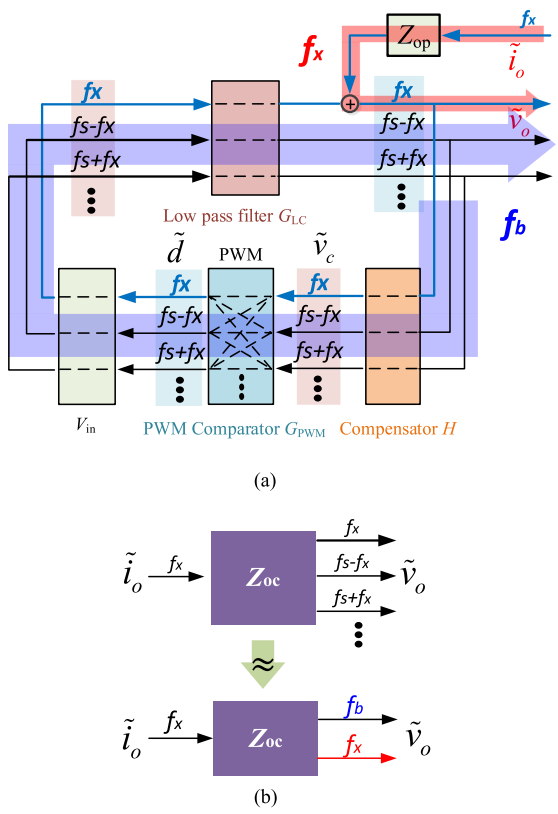

Fig. 18. Simplification of the HSS output impedance matrix model for a voltage-mode-controlled buck converter (see Fig. 14). (a) Multiple frequency coupling in the converter. (b) Model simplification for the multiple frequency components.

C. Reduced-Order HSS Model—Crossed-Frequency Model

The HSS model has a high order because multiple frequency components are involved in the modeling. Fig. 18 shows the simplification process for the HSS output impedance model. In

Fig. 18(a), due to the presence of the low-pass filter and the compensator, the multiple frequency components in the control loop marked by a blue arrow are well attenuated except the low-frequency sideband (defined as f_b; note that f_b could be $f_s - f_x$, $f_x - f_s$, or $2f_s - f_x$; it depends on the value of the perturbation frequency f_x). In addition, the perturbation frequency component f_x goes through the open-loop output impedance to the output voltage without any additional attenuation. Therefore, the multiple frequency components in the output voltage can be approximated by two components, f_b and f_x, as shown in Fig. 18(b). The frequency characteristics in Fig. 17 verify this conclusion.

Based on Fig. 18, a reduced-order HSS model, i.e., a crossed-frequency output impedance matrix model [41], is defined to describe the terminal frequency characteristics of a buck converter, which is

$$\boldsymbol{v_o} = \boldsymbol{Z_{oc}} \times \boldsymbol{i_o}$$

$$\begin{bmatrix} v_o(f_b) \\ v_o(f_x) \end{bmatrix} = \begin{bmatrix} Z_{\rm ocl}(f_b) & Z_{o\rm beat}(f_b) \\ Z_{o\rm beat}(f_x) & Z_{\rm ocl}(f_x) \end{bmatrix} \begin{bmatrix} i_o(f_b) \\ i_o(f_x) \end{bmatrix} \tag{39}$$

where HTF $Z_{\rm ocl}$ is the closed-loop output impedance (same as the result given by describing function), and HTF $Z_{o\rm beat}$ is defined as a beat frequency output impedance describing the crossed-frequency coupling between the low-frequency sideband f_b and the perturbation frequency component f_x.

With the HTF $Z_{o\rm beat}$, the beat frequency oscillations in the phase currents of multiphase voltage regulators caused by some high-frequency repetitive load transients [38], as well as the beat frequency oscillations in a dc nanogrid introduced by the interaction of dc–dc converters with different switching frequencies [39]–[41], can be successfully predicted.

D. Limitations of the Harmonic State-Space Model

With the HSS modeling approach, a multiple-input multiple-output model can be developed to describe the relationship between the perturbation frequency component and the sidebands of the perturbation. The HSS model provides a more accurate frequency-domain description for power electronics circuits, and it successfully predicts the frequency-coupling interactions (e.g., beat frequency oscillations) among multiple converters that both the small-signal averaged model and describing function method fail to do. However, compared with the small-signal averaged model and the describing function method, the HSS model has a higher order, and it increases the modeling complexity significantly. Even, in some cases, a reduced-order HSS model can be derived to simplify the model expression, the reduced-order HSS model is still complex compared with the other two models.

VI. Comparison of Different Modeling Approaches

This section compares the HSS model with the small-signal averaged model and the describing function model through their frequency-domain characteristics and their application on analyzing beat frequency oscillation among multiple converters.

A. Model Comparison Through Frequency-Domain Characteristics

For the converter shown in Fig. 1, according to Section III, the small-signal averaged output impedance model is

$$Z_{\rm ocl-avg} = \frac{Z_{\rm op}(f_x)}{1 + T_{\rm av}(f_x)} \tag{40}$$

where $Z_{\rm op}(f_x)$ is the open-loop output impedance and $T_{\rm avg}(f_x) = G_d(f_x) \cdot G_{\rm PWM} \cdot H(f_x)$ is the loop gain of the small-signal averaged model.

From Section IV, the output impedance describing function model of the converter shown in Fig. 1 is

$$Z_{\rm ocl-df} = \frac{Z_{\rm op}(f_x)}{1 + T_{\rm df}(f_x)} \tag{41}$$

where $T_{\rm df}(f_x)$ is the loop gain of the describing function model defined in (20).

Compared with the HTF matrix defined in (29), the crossed-frequency output impedance matrix model in (39) actually contains two HTFs: one is $Z_{\rm ocl}$ and the other is $Z_{o\rm beat}$. Supposing that the frequency range of interest is $0 < f_x < f_s$, the analytical expressions of the two HTFs $Z_{\rm ocl}$ and $Z_{o\rm beat}$ can be derived from Fig. 18, which are

$$Z_{\rm ocl} = \frac{v_o(f_x)}{i_o(f_x)} = \frac{Z_{\rm op}(f_x)}{1 + \frac{T_{\rm av}(f_x)}{1 + T_{\rm av}(f_b)}} \tag{42}$$

$$Z_{o\rm beat} = \frac{v_o(f_b)}{i_o(f_x)} = \frac{Z_{\rm op}(f_x) \cdot H(f_x) \cdot G_{\rm LC}(f_b)}{1 + T_{\rm av}(f_x) + T_{\rm av}(f_b)} \cdot \frac{V_{\rm in}}{V_m} \cdot e^{j2D\pi}. \tag{43}$$

According to the analytical expressions defined from (40) to (43) and the parameters listed in Table I, the frequency-domain characteristics of these models can be plotted, which is shown in Fig. 19.

The small-signal averaged output impedance $Z_{\rm ocl-avg}$ in (40) and the output impedance describing function $Z_{\rm ocl-df}$ in (41) have different expressions because of their different loop gains. From Fig. 11, the two loop gains $T_{\rm avg}$ and $T_{\rm df}$ are similar in low-frequency regions. In high-frequency regions, they are quite different, but their values are both very small compared with "1" in (40) and (41). Therefore, the output impedances derived from the small-signal averaged model and the describing function method are almost the same in the whole frequency range of interest.

The HTF $Z_{\rm ocl}$ in (42) is the same as the describing function $Z_{\rm ocl-df}$ in (41). Compared with the describing function method, the reduced HSS model adds a new function: the HTF $Z_{o\rm beat}$ defined in (43). It can be seen from Fig. 19 that the HTF $Z_{o\rm beat}$ is small enough to be ignored in low-frequency regions, but it should be considered around switching frequency. The facts indicate that the SISO describing function model is no longer effective to describe the output-current-to-output-voltage relationship around switching frequency in some cases.

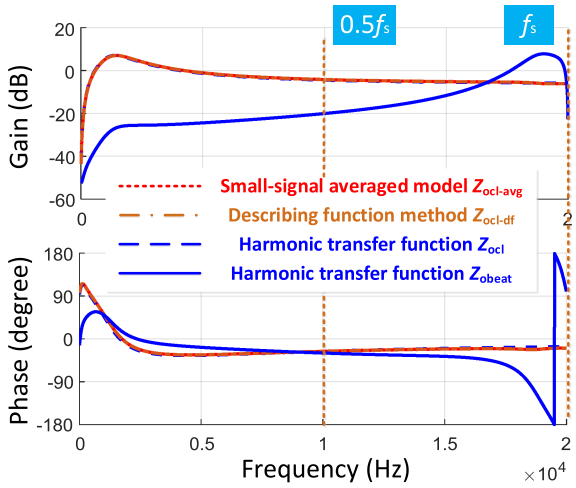

Fig. 19. Frequency characteristics of four HTFs of the closed-loop output impedance.

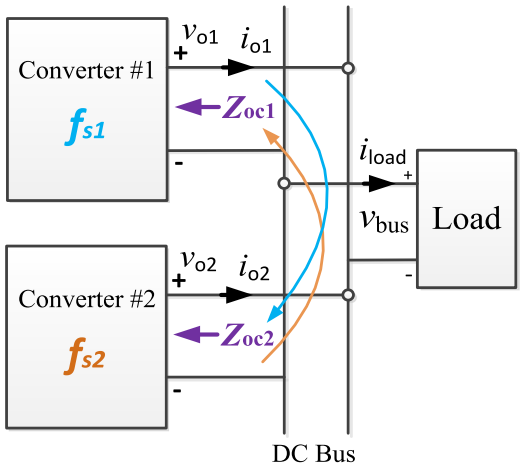

Fig. 20. Two power converters in parallel.

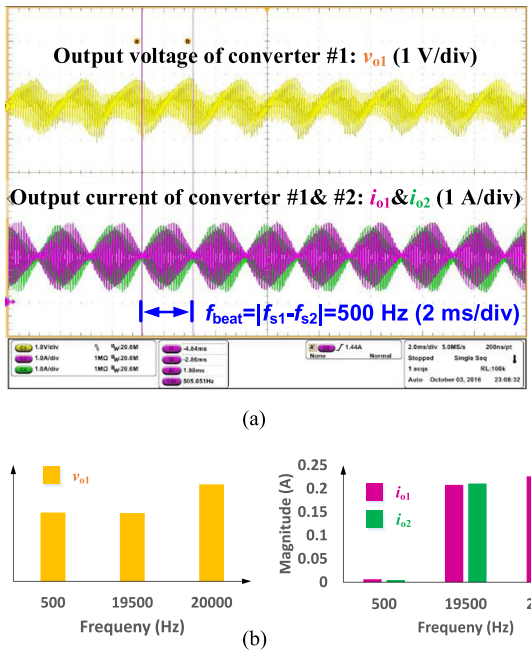

Fig. 21. Waveforms when $f_{s1} = 20$ kHz and $f_{s2} = 19.5$ kHz. (a) Time-domain waveforms. (b) FFT results.

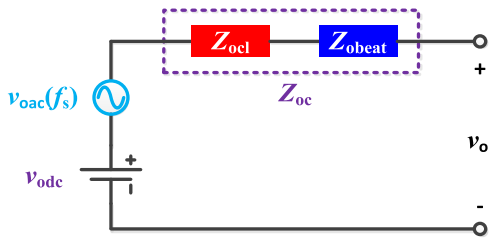

Fig. 22. Equivalent circuit model for a power converter.

B. Model Application—Beat Frequency Oscillation Analysis

Fig. 20 shows a system consisting of two power converters in parallel, where f_{s1} and f_{s2} are their switching frequencies, and $Z_{\rm oc1}$ and $Z_{\rm oc2}$ are output impedances of the two converters. In this system, one converter's output switching ripple is the other converter's perturbation. In a real system that consists of two dc–dc converters in parallel, when converter #1 is set to $f_{s1} = 20$ kHz and converter #2 is set to $f_{s2} = 19.5$ kHz, the time-domain waveforms for the output voltage of converter #1 v_{o1}, the output currents of both converter #1 i_{o1} and converter #2 i_{o2}, are shown in Fig. 21(a). The corresponding fast Fourier transformation (FFT) results are shown in Fig. 21(b) [41].

Since the 500-Hz component in Fig. 21 is an additional frequency component, the SISO models (i.e., the small-signal averaged model and the describing function model) fail to predict this kind of oscillation. However, according to the crossed-frequency model, the beat frequency oscillation can be explained and predicted accurately [41].

Fig. 22 shows an equivalent circuit model for buck converters based on the crossed-frequency output impedance matrix model defined in (39). With the equivalent circuit in Fig. 22, an equivalent circuit model for the parallel system (see Fig. 20) is shown in Fig. 23, where $Z_{\rm cab}$ represents the cable impedance.

It can be seen from Fig. 23 that the switching harmonics of one converter have an effect on the beat frequency output impedance of the other converter. Such kind of interaction finally leads to a beat frequency oscillation in the circuit. In contrast, if the averaged small-signal model or describing function model is applied to do the analyses shown in Figs. 22 and 23, then no beat frequency oscillation will be obtained because both the averaged small-signal model and the describing function model are SISO models without the beat frequency output impedance. Therefore, to predict the frequency-coupling interactions (e.g., beat frequency oscillations) among multiple power converters, the crossed-frequency (or HSS) model in the MIMO form is required.

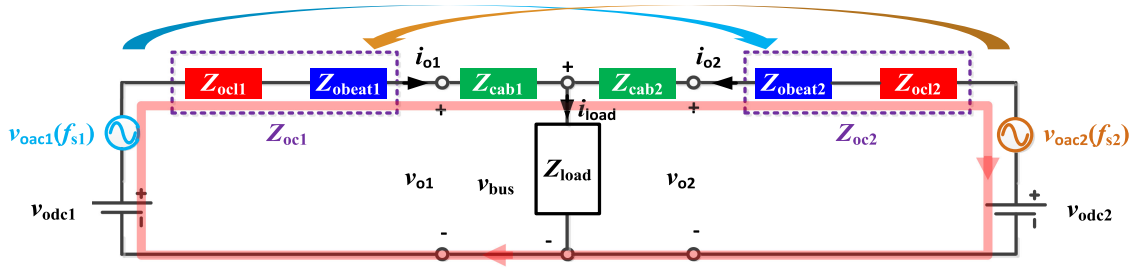

Fig. 23. Equivalent circuit diagram for the system in Fig. 20.

TABLE II
COMPARISON OF DIFFERENT SMALL-SIGNAL MODELING METHODS

	Small-signal averaged models	Describing function based models	HSS models
Theoretical foundation	Linearization at an equilibrium point	Harmonic linearization	Trajectory linearization and LTP theory
Model form	SISO model	SISO model	MIMO
Sideband effect	Ignored	Considered	Considered
Effective frequency range	Low frequency region	Both low and high frequency regions	Both low and high frequency regions
Model order	Low	Medium	High
Main application areas	Controller design and stability analysis	Loop gain phase delay and subharmonic oscillation	Beat frequency oscillation and large system simulation

VII. CONCLUSION

This paper reviews and compares different small-signal modeling approaches used in power electronics from the following aspects: theoretical foundation, model form, sideband effect, effective frequency range, model order, and application areas. Table II summarizes the comparison results. The small-signal averaged models are SISO LTI models derived through the linearization at an equilibrium point. They are good tools for controller design and stability analysis in the low-frequency region, but their accuracy becomes questionable at high frequencies. The describing function models are derived from harmonic linearization, and they are also SISO models, but they consider the sideband effect and improve the modeling accuracy at high frequency. The describing function models are effective for individual power converters at higher frequencies but questionable to analyze the high-frequency interaction of multiple converters in series or in parallel (e.g., beat frequency oscillations). HSS models are obtained by the linearization at a time-periodic trajectory and the theory of the LTP system and HSS. They are MIMO LTI models, which describe the reference input to the responded output not only from perturbation frequency to perturbation frequency, but also from perturbation frequency to sidebands. HSS models apply for both individual converters and system with multiple converters at both low and high frequencies. However, the order of HSS models is high, so normally reduced-order models, i.e., crossed-frequency models, are required for real applications.

REFERENCES

[1] D. Boroyevich, I. Cvetković, D. Dong, R. Burgos, F. Wang, and F. C. Lee, "Future electronic power distribution systems a contemplative view," in *Proc. 12th Int. Conf. Optim. Elect. Electron. Equip.*, Basov, Romania, 2010, pp. 1369–1380.

[2] F. Blaabjerg, Y. Yang, D. Yang, and X. Wang, "Distributed power-generation systems and protection," *Proc. IEEE*, vol. 105, no. 7, pp. 1311–1331, Jul. 2017.

[3] N. Flourentzou, V. G. Agelidis, and G. D. Demetriades, "VSC-based HVDC power transmission systems: An overview," *IEEE Trans. Power Electron.*, vol. 24, no. 3, pp. 592–602, Mar. 2009.

[4] J. G. Kassakian, M. F. Schlecht, and G. C. Verghese, *Principles of Power Electron*. Reading, MA, USA: Addison-Wesley, 1991.

[5] G. C. Verghese, M. E. Elbuluk, and J. G. Kassakian, "A general approach to sampled-data modeling for power electronic circuits," *IEEE Trans. Power Electron.*, vol. PE-1, no. 2, pp. 76–89, Apr. 1986.

[6] A. R. Brown, "Sampled-data modeling of switching regulators," in *Proc. IEEE Power Electron. Spec. Conf.*, Boulder, CO, USA, 1981, pp. 349–369.

[7] D. Maksimovic, A. M. Stankovic, V. J. Thottuvelil, and G. C. Verghese, "Modeling and simulation of power electronic converters," *Proc. IEEE*, vol. 89, no. 6, pp. 898–912, Jun. 2001.

[8] G. W. Wester and R. D. Middlebrook, "Low Frequency characterization of switched dc-to-dc converters," in *Proc. IEEE Power Electron. Spec. Conf.*, 1972, pp. 9–20.

[9] R. D. Middlebrook and S. Cuk, "A general unified approach to modeling switching converter power stages," in *Proc. IEEE Power Electron. Spec. Conf.*, 1976, pp. 18–34.

[10] R. D. Middlebrook, "Small-signal modeling of pulse-width modulated switched-mode power converters," *Proc. IEEE*, vol. 76, no. 4, pp. 343–354, Apr. 1988.

[11] N. N. Bogoliubov and Y. A. Mitropolsky, *Asymptotic Methods in the Theory of Nonlinear Oscillations*. New Delhi, India: Hindustan Publishing, 1961.

[12] R. M. Bass, "Large-signal tools for power electronics: State-space analysis and averaging theory," Ph.D. dissertation, Dept. Elect. Comput. Eng., Univ. Illinois Urbana–Champaign, Champaign, IL, USA, 1990.

[13] P. T. Krein, J. Bentsman, R. M. Bass, and B. L. Lesieutre, "On the use of averaging for the analysis of power electronic systems," *IEEE Trans. Power Electron.*, vol. 5, no. 2, pp. 182–190, Apr. 1990.
[14] B. Lehman and R. M. Bass, "Switching frequency dependent averaged models for PWM DC-DC converters," *IEEE Trans. Power Electron.*, vol. 11, no. 1, pp. 89–98, Jan. 1996.
[15] S. R. Sanders, J. M. Noworolski, X. Z. Liu, and G. C. Verghese, "Generalized averaging method for power conversion circuits," *IEEE Trans. Power Electron.*, vol. 6, no. 2, pp. 251–259, Apr. 1991.
[16] V. A. Caliskan, O. C. Verghese, and A. M. Stankovic, "Multifrequency averaging of DC/DC converters," *IEEE Trans. Power Electron.*, vol. 14, no. 1, pp. 124–133, Jan. 1999.
[17] A. M. Stankovic, S. R. Sanders, and T. Aydin, "Dynamic phasors in modeling and analysis of unbalanced polyphase AC machines," *IEEE Trans. Energy Convers.*, vol. 17, no. 1, pp. 107–113, Mar. 2002.
[18] R. M. Bass and J. Sun, "Large-signal averaging methods under large ripple conditions [for power convertors]," in *Proc. 29th Annu. IEEE Power Electron. Spec. Conf.*, Fukuoka, Japan, 1998, vol. 1, pp. 630–632.
[19] W. S. Levine, *Control System Fundamentals*. Boca Raton, FL, USA: CRC Press, 2000.
[20] A. Packard, K. Poolla, and R. Horowitz, "Dynamic systems and feedback class notes," Dept. Mech. Eng., Univ. California, Berkeley, CA, USA, Spring 2005.
[21] Z. Vukic, *Nonlinear Control Systems*. Boca Raton, FL, USA: CRC Press, 2003.
[22] Y. Liu, X. Wu, J. J. Zhu, and J. Lew, "Omni-directional mobile robot controller design by trajectory linearization," in *Proc. Amer. Control Conf.*, 2003, vol. 4, pp. 3423–3428.
[23] M. C. Mickle, R. Huang, and J. J. Zhu, "Unstable, nonminimum phase, nonlinear tracking by trajectory linearization control," in *Proc. IEEE Int. Conf. Control Appl.*, vol. 1, 2004, pp. 812–818.
[24] A. Gelb and W. E. Vander Velde, *Multiple-Input Describing Functions and Nonlinear System Design*. New York, NY, USA: McGraw Hill, 1968.
[25] J. Sun and K. J. Karimi, "Small-signal input impedance modeling of line-frequency rectifiers," *IEEE Trans. Aerosp. Electron. Syst.*, vol. 44, no. 4, pp. 1489–1497, Oct. 2008.
[26] L. Jian, "Current-Mode control: Modeling and its digital application," Ph.D. dissertation, Dept. Elect. Eng., Virginia Tech, Blacksburg, VA, USA, 2009.
[27] Y. Qiu, M. Xu, K. Yao, J. Sun, and F. C. Lee, "Multi-frequency small-signal model for Buck and multi-phase Buck converters," *IEEE Trans. Power Electron.*, vol. 21, no. 5, pp. 1185–1192, Sep. 2006.
[28] Y. Qiu, M. Xu, J. Sun, and F. C. Lee, "A generic high-frequency model for the nonlinearities in buck converters," *IEEE Trans. Power Electron.*, vol. 22, no. 5, pp. 1970–1977, Sep. 2007.
[29] R. D. Middlebrook, "Topics in multiple-loop regulators and current mode programming," in *Proc. IEEE Power Electron. Spec. Conf.*, 1985, pp. 716–732.
[30] F. C. Lee, Y. Yu, and M. F. Mahmoud, "A unified analysis and design procedure for a standardized control module for DC-DC switching regulators," in *Proc. IEEE Power Electron. Spec. Conf.*, 1980, pp. 284–301.
[31] R. D. Middlebrook, "Modeling current-programmed buck and boost regulators," *IEEE Trans. Power Electron.*, vol. 4, no. 1, pp. 36–52, Jan. 1989.
[32] D. J. Packard, "Discrete modeling and analysis of switching regulators," Ph.D. dissertation, Dept. Elect. Eng., California Inst. Technol., Pasadena, CA, USA, May 1976.
[33] R. B. Ridley, "A new, continuous-time model for current-mode control," *IEEE Trans. Power Electron.*, vol. 6, no. 2, pp. 271–280, Apr. 1991.
[34] J. Li and F. C. Lee, "New modeling approach and equivalent circuit representation for current mode control," *IEEE Trans. Power Electron.*, vol. 25, no. 5, pp. 1218–1230, May 2010.
[35] Y. Yan, F. C. Lee, and P. Mattavelli, "Unified three-terminal switch model for current mode controls," *IEEE Trans. Power Electron.*, vol. 27, no. 9, pp. 4060–4070, Sep. 2012.
[36] Y. Yan, F. C. Lee, P. Mattavelli, and S. Tian, "Small signal analysis of V^2 control using equivalent circuit model of current mode controls," *IEEE Trans. Power Electron.*, vol. 31, no. 7, pp. 5344–5353, Jul. 2016.
[37] S. Tian, F. C. Lee, Q. Li, and Y. Yan, "Unified equivalent circuit model and optimal design of V^2 controlled buck converters," *IEEE Trans. Power Electron.* vol. 31, no. 2, pp. 1734–1744, Feb. 2016.
[38] J. Sun, Y. Qiu, M. Xu, and F. C. Lee, "High-Frequency dynamic current sharing analyses for multiphase buck VRs," *IEEE Trans. Power Electron.*, vol. 22, no. 6, pp. 2424–2431, Nov. 2007.
[39] X. Yue, Y. Zhu, S. Yang, Y. Chen, F. Zhuo, and Y. Pei, "A modulation and sampling based modeling method for the nonlinearities of power converters and its application analysis," in *Proc. 17th Eur. Conf. Power Electron. Appl.*, Geneva, Switzerland, 2015, pp. 1–10.
[40] X. Yue, F. Zhuo, S. Yang, Y. Pei, and H. Yi, "A matrix-based multifrequency output impedance model for beat frequency oscillation analysis in distributed power systems," *IEEE J. Emerg. Sel. Topics Power Electron.*, vol. 4, no. 1, pp. 80–92, Mar. 2016.
[41] X. Yue, D. Boroyevich, F. C. Lee, F. Chen, R. Burgos, and F. Zhuo, "Beat frequency oscillation analysis for power electronic converters in DC nanogrid based on crossed frequency output impedance matrix model," *IEEE Trans. Power Electron.*, vol. 33, no. 4, pp. 3052–3064, Apr. 2018.
[42] E. Mollerstedt and B. Bernhardsson, "Out of control because of harmonics—An analysis of the harmonic response of an inverter locomotive," *IEEE Control Syst.*, vol. 20, no. 4, pp. 70–81, Aug. 2000.
[43] G. N. Love and A. R. Wood, "Harmonic state-space model of power electronics," in *Proc. 13th Int. Conf. Harmon. Qual. Power*, 2008, pp. 1–6.
[44] M. S.-P. Hwang and A. R. Wood, "A new modelling framework for power supply networks with converter based loads and generators—The harmonic state-space," in *Proc. IEEE Int. Conf. Power Syst. Technol.*, 2012, pp. 1–6.
[45] J. B. Kwon, X. Wang, F. Blaabjerg, and C. L. Bak, "Frequency domain modeling and simulation of DC power electronic systems," *IEEE Trans. Power Electron.*, vol. 32, no. 2, pp. 1044–1055, Feb. 2017.
[46] N. M. Wereley, "Analysis and control of linear periodically time varying systems," Ph.D. dissertation, Dept. Aeronaut. Astronaut., Massachusetts Inst. Technol., Cambridge, MA, USA, 1990.
[47] N. M. Wereley and S. R. Hall, "Linear time periodic systems: Transfer function, poles, transmission zeroes and directional properties," in *Proc. Amer. Control Conf.*, 1991, pp. 1179–1184.
[48] N. M. Wereley and S. R. Hall, "Frequency response of linear time periodic systems," in *Proc. IEEE 29th Conf. Decis. Control*, 1990, vol. 6, pp. 3650–3655.
[49] X. Yue, X. Wang, F. Blaabjerg, D. Boroyevich, R. Burgos, and F. Lee, "Wideband small-signal input dq admittance modeling of six-pulse diode rectifiers," in *Proc. IEEE Appl. Power Electron. Conf. Expo.*, San Antonio, TX, USA, 2018, pp. 1981–1988.
[50] X. Yue, D. Boroyevich, R. Burgos, and F. Zhuo, "Modeling and analysis for input characteristics of line-frequency rectifiers," in *Proc. IEEE Energy Convers. Congr. Expo.*, Milwaukee, WI, USA, 2016, pp. 1–8.
[51] J. Sun and H. Liu, "Sequence impedance modeling of modular multilevel converters," *IEEE J. Emerg. Sel. Topics Power Electron.*, vol. 5, no. 4, pp. 1427–1443, Dec. 2017.
[52] A. V. Oppenheim, A. S. Willsky, and S. H. Nawab, *Signals and Systems*, vol. 2. Englewood Cliffs, NJ, USA: Prentice-Hall, 1983.
[53] R. Tymerski, V. Vorperian, F. C. Lee, and W. T. Baumann, "Nonlinear modeling of the PWM switch," *IEEE Trans. Power Electron.*, vol. 4, no. 2, pp. 225–233, Apr. 1989.
[54] V. Vorperian, "Simplified analysis of PWM converters using model of PWM switch. Continuous conduction mode," *IEEE Trans. Aerosp.*, vol. 26, no. 3, pp. 490–496, May 1990.
[55] M. D. Greenberg, *Advanced Engineering Mathematics*. Englewood Cliffs, NJ, USA: Prentice-Hall, 1988.

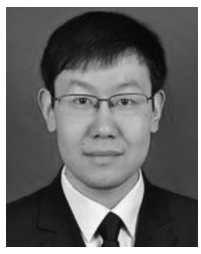

Xiaolong Yue (S'12–M'17) received the bachelor's and Ph.D. degrees in electrical engineering from Xi'an Jiaotong University (XJTU), Xi'an, China, in 2011 and 2017, respectively.

From 2011 to 2017, he was a Research Assistant with XJTU. From 2015 to 2016, he was a Visiting Ph.D. Student with the Center for Power Electronics Systems, Virginia Tech, VA, USA. From 2017 to 2018, he was a Postdoctoral Fellow with the Department of Energy Technology, Aalborg University, Aalborg East, Denmark. Since 2018, he has been a Power Design Engineer with Ericsson AB, Gothenburg, Sweden. His research interests include stability of ac and dc power systems, modeling and control of power electronics converters and systems, and impedance measurement of power-electronic-based systems.

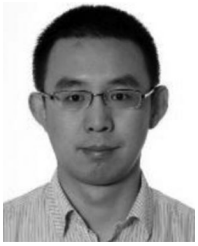

Xiongfei Wang (S'10–M'13–SM'17) received the B.S. degree from Yanshan University, Qinhuangdao, China, in 2006, the M.S. degree from the Harbin Institute of Technology, Harbin, China, in 2008, both in electrical engineering, and the Ph.D. degree in energy technology from Aalborg University, Aalborg, Denmark, in 2013.

Since 2009, he has been with Aalborg University, where he is currently an Associate Professor with the Department of Energy Technology. His research interests include modeling and control of grid-connected converters, harmonics analysis and control, passive and active filters, and stability of power-electronic-based power systems.

Dr. Wang is an Associate Editor for the IEEE TRANSACTIONS ON POWER ELECTRONICS, the IEEE TRANSACTIONS ON INDUSTRY APPLICATIONS, and the IEEE JOURNAL OF EMERGING AND SELECTED TOPICS IN POWER ELECTRONICS. He is also the Guest Editor for the Special Issue "Grid-Connected Power Electronics Systems: Stability, Power Quality, and Protection" in the IEEE TRANSACTIONS ON INDUSTRY APPLICATIONS. He was a recipient of the Second Prize Paper Award and the Outstanding Reviewer Award of the IEEE TRANSACTIONS ON POWER ELECTRONICS in 2014 and 2017, respectively, the Second Prize Paper Award of the IEEE TRANSACTIONS ON INDUSTRY APPLICATIONS in 2017, and the Best Paper Awards at the 2016 IEEE International Symposium on Power Electronics for Distributed Generation Systems and the 2017 IEEE Power and Energy Society General Meeting. In 2018, he was a recipient of the IEEE Power Electronics Society Richard M. Bass Outstanding Young Power Electronics Engineer Award.

Frede Blaabjerg (S'86–M'88–SM'97–F'03) received the Ph.D. degree in electrical engineering from Aalborg University, Aalborg, Denmark, in 1995.

He was with ABB-Scandia, Randers, Denmark, from 1987 to 1988. He became an Assistant Professor in 1992, an Associate Professor in 1996, and a Full Professor of power electronics and drives in 1998 with Aalborg University. In 2017, he became a Villum Investigator. He is Honoris Causa with the University Politehnica Timisoara, Romania, and Tallinn Technical University, Estonia. He has authored or coauthored more than 500 journal papers in the fields of power electronics and its applications. He is the coauthor of two monographs and editor of seven books in power electronics and its applications. His current research interests include power electronics and its applications such as in wind turbines, photovoltaic systems, reliability, harmonics, and adjustable speed drives.

Dr. Blaabjerg is a recipient of 26 IEEE Prize Paper Awards, the IEEE Power Electronics Society (PELS) Distinguished Service Award in 2009, the EPE-PEMC Council Award in 2010, the IEEE William E. Newell Power Electronics Award 2014, and the Villum Kann Rasmussen Research Award 2014. He was the Editor-in-Chief of the IEEE TRANSACTIONS ON POWER ELECTRONICS from 2006 to 2012. He was a Distinguished Lecturer for the IEEE Power Electronics Society from 2005 to 2007 and for the IEEE Industry Applications Society from 2010 to 2011 as well as 2017 to 2018. In 2018, he is the President Elect of the IEEE PELS. He is nominated in 2014, 2015, 2016, and 2017 by Thomson Reuters to be among the most 250 cited researchers in Engineering in the world. In 2017, he became Honoris Causa with the University Politehnica Timisoara, Romania.